

High cycle fatigue of a die cast AZ91E-T4 magnesium alloy

M.F. Horstemeyer^{a,*}, N. Yang^b, Ken Gall^c, D.L. McDowell^d, J. Fan^e, P.M. Gullett^b

^a Department of Mechanical Engineering, Mississippi State University, 206 Carpenter Bldg, Mississippi State, MS 39762, USA

^b Center for Materials and Engineering Sciences, Sandia National Laboratories, Livermore, CA 94550, USA

^c Department of Mechanical Engineering, University of Colorado, Boulder, CO 80309, USA

^d George Woodruff School of Mechanical Engineering, Georgia Institute of Technology, Atlanta, GA 30332, USA

^e Department of Mechanical Engineering, Alfred University, Alfred, NY, USA

Received 3 July 2003; accepted 11 November 2003

Abstract

This study reveals the micro-mechanisms of fatigue crack nucleation and growth in a commercial high-pressure die cast automotive AZ91E-T4 Mg component. Mechanical fatigue tests were conducted under $R = -1$ conditions on specimens machined at different locations in the casting at total strain amplitudes ranging from 0.02% to 0.5%. Fracture surfaces of specimens that failed in the high cycle fatigue regime with lives spanning two orders of magnitude were examined using a scanning electron microscope. The difference in lives for the Mg specimens was primarily attributed to a drastic difference in nucleation site sizes, which ranged from several hundred μm 's to several mm's. A secondary effect may include the influence of average secondary dendrite arm spacing and average grain size. At low crack tip driving forces ($K_{\text{max}} < 3.5 \text{ MPa} \sqrt{\text{m}}$) intact particles and boundaries act as barriers to fatigue crack propagation, and consequently the cracks tended to avoid the interdendritic regions and progress through the cells, leaving a fine striated pattern in this single-phase region. At high driving forces ($K_{\text{max}} > 3.5 \text{ MPa} \sqrt{\text{m}}$) fractured particles and boundary decohesion created weak paths for fatigue crack propagation, and consequently the cracks followed the interdendritic regions, leaving serrated markings as the crack progressed through this heterogeneous region. The ramifications of the results on future modeling efforts are discussed in detail. © 2003 Acta Materialia Inc. Published by Elsevier Ltd. All rights reserved.

Keywords: Fatigue; Magnesium; Porosity; Micromechanisms; Crack propagation

1. Introduction

A recent push by the automotive industry to lower the fuel consumption and cost of production automobiles is providing enhanced motivation for the study of lightweight cast materials for structural components. Cast materials have clear economic advantage compared to wrought materials for mass production of components due to their lower long-term processing and assembly costs. On the other hand, processing related variability of monotonic and fatigue properties curtail the potential advantage of cast materials. Although cast and wrought materials can often have comparable maximum properties, cast materials typically show considerably more scatter in fatigue and monotonic properties. Consequently, castings have typically been

designed by a worst-case-scenario paradigm, whereby the component is assumed to have the weakest material in the location of the highest stresses. Such an approach leads to over-designed components with material placed in unnecessary regions of the casting. The variability in the properties of as-cast materials is a direct consequence of the extremely strong dependence of the resulting microstructure on local solidification mechanisms. For example, the dimensions of the casting dictate the local cooling rate, which in turn produces a geometry dependent dendrite cells size and porosity level. A more robust design methodology for cast components would entail predicting the distribution of critical microstructural parameters as a function of the geometry of the casting, followed by life estimation based on the predicted microstructural features.

To facilitate the interactive microstructure-based design of cast components for long life behavior, the mechanisms of fatigue and the sources of variability

* Corresponding author. Fax: +1-662-325-7223.

E-mail address: mforst@me.msstate.edu (M.F. Horstemeyer).

must be linked to critical microstructural features in the as-cast material. The present study examines the links between fatigue mechanisms and microstructure in cast magnesium (Mg) alloys, which have found a myriad of applications in industry [1–3]. The low density of Mg alloys combined with their reasonable cost, strength, and machining capacity make them attractive for numerous structural applications. On the contrary, a disadvantage of cast Mg based alloys is their relatively poor corrosion resistance. Ongoing work [4–6] in the area of corrosion has focused on linking the corrosion performance to microstructural constituents in cast Mg in an effort to help design corrosion resistant materials. Emerging processing studies have also improved our understanding of the links between the solidification variables and as-cast microstructures in Mg alloys [7]. Commensurate with the evolution of knowledge and material behavior in the areas of corrosion and solidification, fatigue-microstructure relationship in cast Mg alloys must also be analyzed.

Previous work focusing on the mechanical behavior of cast Mg has examined the monotonic [7–14], high-temperature creep [9,10], and cyclic [15–18] properties of cast Mg alloys. These fundamental studies have proven that the properties of cast Mg depend very strongly on the processing conditions; however, a link to microstructure is often not made, particularly under cyclic loading conditions. For example, one study has outlined the relationship between microstructure and local fracture mechanisms under monotonic loading [13], but such information is not available for fatigue loading conditions in die cast AZ91 materials. Most previous work on the fatigue of cast Mg has focused on the application of macroscopic empirical fatigue life correlations [17,18] or on the effects of mechanical alloying on fatigue resistance [16]. To significantly build upon these initial fatigue studies, the micro-mechanisms of fatigue in cast Mg alloys must be examined. Given information on the critical micro-mechanisms of fatigue crack formation and growth, modeling capabilities can be developed that can predict fatigue life and variability as a function of the microstructure.

In the present study fatigue mechanisms in cast AZ91E-T4 magnesium are examined. The specimens used for the fatigue study were machined from different locations of a commercial high-pressure die cast automobile component. Mechanical fatigue tests were conducted under $R = -1$ conditions and constant total

strain amplitudes varying from 0.02% to 0.5%. The high cycle fatigue (HCF) lives of the specimens were discovered to vary by several orders of magnitude. The fracture surfaces and grip regions of selected specimens cycled until failure under HCF conditions were examined with scanning electron microscope (SEM) and optical microscopy. The purpose of the microscopy was to determine the role of the microstructure on fatigue crack nucleation and subsequent fatigue crack growth. Particular emphasis was placed on elucidating the nucleation sites and microstructural paths of fatigue cracks during different stages of the specimen life. Following the presentation of the experimental results, the ramifications on the future of prediction and prevention of fatigue in die-cast AZ91E-T4 alloys is discussed.

2. Materials and methods

The composition of the AZ91E-T4 cast magnesium employed for the present study is shown in Table 1. Small fatigue specimens with a 3 mm × 7 mm rectangular gage cross section were extracted from a commercial high-pressure automotive die cast component. The details of the casting process are proprietary. However, the as-cast microstructure in the grip (undeformed) section of selected test specimens was examined, since the purpose of this study is to link microstructural features to fatigue mechanisms. The dependence of microstructural features on casting parameters is beyond the scope of this study, but has been recently documented [8]. Constant amplitude fatigue tests were conducted in strain control at total strain amplitudes ranging from 0.02% to 0.5% ($R = -1$, frequency = 0.5 Hz) on the machined specimens. The tests were conducted in laboratory air at a temperature of 25 °C. After cyclic saturation in the fatigue tests, the machine feedback mode was switched to load control and the frequency was increased to 10 Hz.

The undeformed microstructure was examined with an optical microscope and SEM. Undeformed microstructural specimens were extracted from the grip section of selected specimens and were examined in the as-polished and etched states. A Nital etchant was used to elucidate the grain boundaries and solidification induced dendrite structures within the grains. The average secondary dendrite arm spacing in undeformed samples was estimated by measuring the spacing at about ten

Table 1
Composition of AZ91E cast magnesium

Mg	Al	Zn	Mn	Si	Fe	Cu	Ni	Other
Balance	8.1–9.3	0.40–1.0	0.17–0.35	0.20	0.005	0.015	0.001	0.01 (0.30)
				Max	Max	Max	Max	Max total (each)

Values in percent.

spatial locations throughout the specimen and then averaging the results. The average grain size was estimated by averaging the size of grains on the specimen cross section.

Local fatigue mechanisms were evaluated by examining the fracture surfaces of samples with the SEM using either secondary electron imaging (SEI) or backscatter electron imaging (BEI). When information containing the spatial arrangement of a particular phase was required, BEI was used. BEI differs from SEI in that contrast depends on the atomic mass of the constituent elements of a particular phase. Because of this, phases comprised of higher atomic mass elements create more backscatter electrons and thus appear brighter on the SEM image. Energy dispersive X-ray (EDX) analysis was used to determine the phases present in SEM samples.

3. Experimental results

3.1. Fatigue tests

Total strain amplitude versus cycles to failure data from 34 AZ91E-T4 Mg specimens are presented in Fig. 1. The variability in the fatigue life of the small specimens exceeds two orders of magnitude for a given applied strain in the HCF regime. The variability in the fatigue life data in the low cycle fatigue regime is less severe, although still one order of magnitude on life. The smooth function of the maximum life as a function of applied strain amplitude may represent the limit to which microstructural refinement will improve fatigue properties in cast AZ91 Mg.

Four representative samples loaded at HCF amplitudes of 0.10% and 0.075% in Fig. 2 were chosen for analysis, and are designated as Samples S1 (0.075%), S2

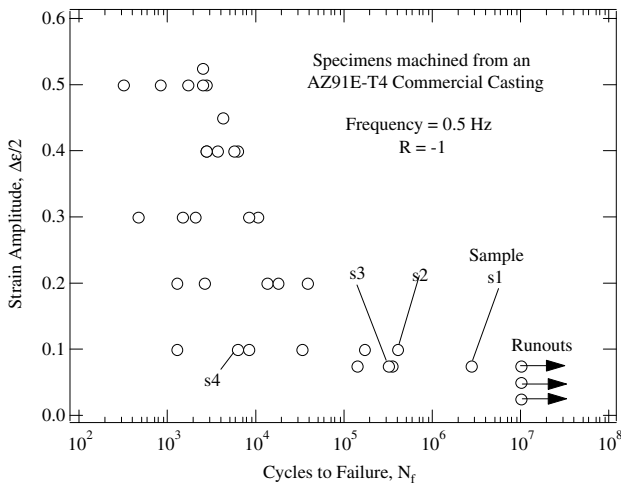


Fig. 1. Strain-life curve of AZ91E-T4 magnesium alloy.

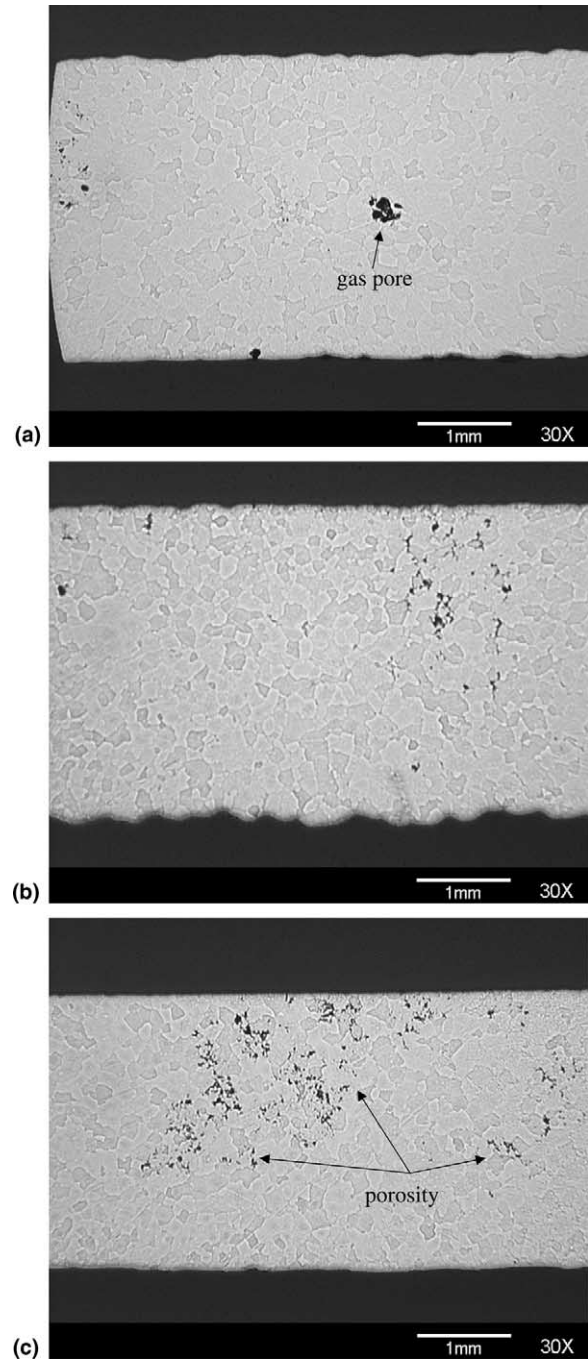


Fig. 2. (a) Optical images from a polished cross section of the grip section of sample S1 shows gas pore and illustrates dendrite morphology. (b) Optical images from a polished cross section of the grip section of sample S3 shows porosity and illustrates a similar dendrite morphology to that of S1. (c) Optical images from a polished cross section of the grip section of sample S4 shows more porosity than S1 and S3 but illustrates a similar dendrite morphology.

(0.10%), S3 (0.075%), and S4 (0.10%). To elucidate the microstructures and fatigue mechanisms that lead to the distinctly different fatigue lives, selected samples with numbers of cycles to failure that vary within two orders of magnitude in terms of life had been selected. In the

sections that follow, the grip section microstructure and fracture surfaces of the Samples S1–S4 are presented.

3.2. Cast microstructure

The as-cast microstructures of samples S1, S3, and S4 are shown in Fig. 2–4. Fig. 2 shows optical images from a polished cross section of the grip section of samples (a)

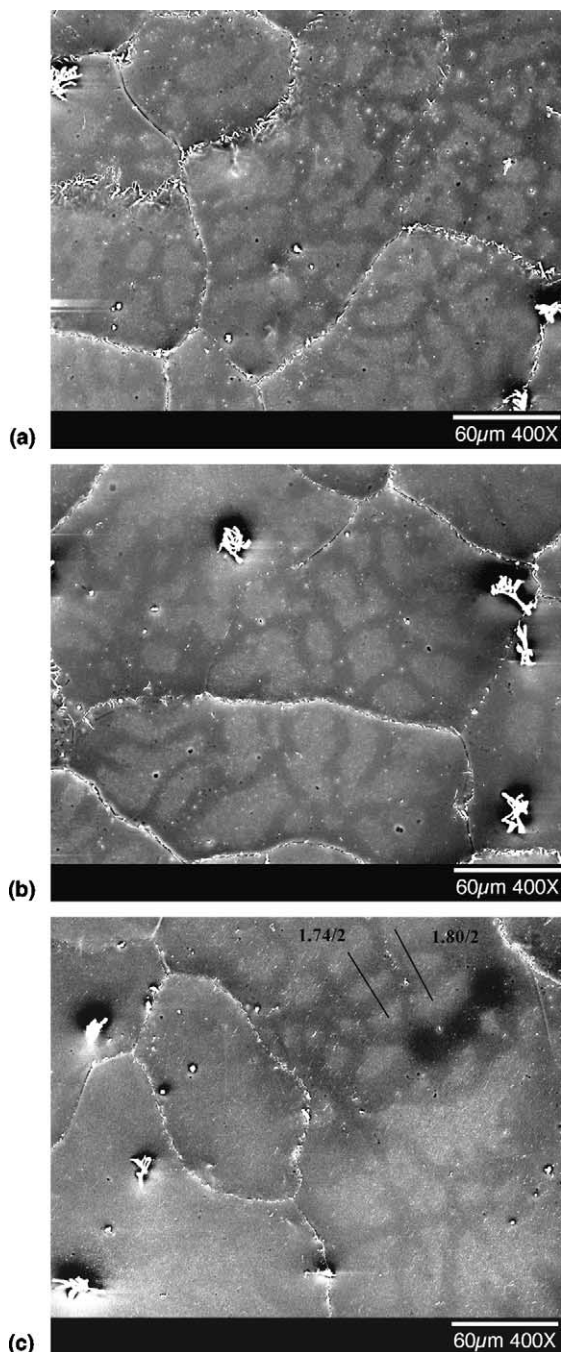


Fig. 3. Etched secondary SEM images of the microstructure from the grip section of samples (a) S1, (b) S3, and (c) S4. The high contrast images highlight the dendrite structure within the grains. The white flakes are AlMnSi particles protruding from the specimen surface.

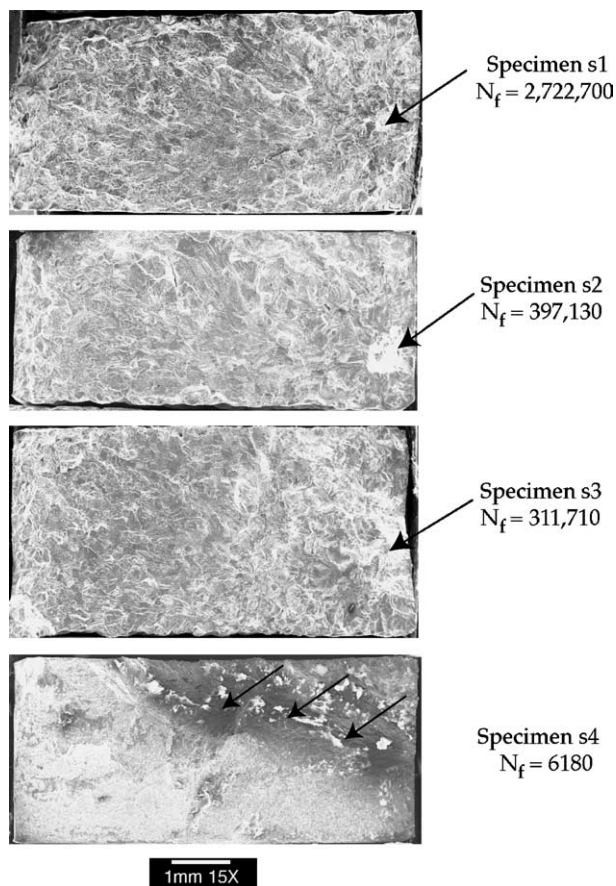


Fig. 4. Overall fracture surfaces of samples S1–S4. The location of the fatigue crack formation sites are indicated by arrows.

S1, (b) S3, and (c) S4. The low magnification optical images in Fig. 2 highlight porosity and the granular structure of the cast specimens. The volume fraction of porosity is more severe as the sample number increases from S1 to S4. The average grain size as measured from the images of samples S1, S3, and S4 in Fig. 2 also increases as the sample number increases (Table 2).

The samples used for optical imaging in Fig. 2 were etched to reveal additional microstructural features caused by the solidification of the casting. Fig. 3 shows high contrast SEM images of samples S1, S3, and S4 after etching. The etching reveals a dendritic structure within the grains. Based on the Mg–Al phase diagram, AZ91 Mg should contain α -Mg with trace solid solution Al and β -Al₁₂Mg₁₇. The dendrite cells are composed of

Table 2
Measured average grain size and secondary dendrite arm spacing for selected cast Mg specimens

	Sample S1	Sample S3	Sample S4
Average grain size (μm)	105	110	140
Average secondary dendrite arm spacing (μm)	14.7	21.5	22.1

pre-eutectic α -Mg while the interdendritic arms are decorated by the eutectic β particles within a eutectic α -Mg. The average secondary dendrite arm spacing of the different samples was determined by making multiple measurements with traversing lines as indicated on Fig. 3(c). The average secondary dendrite arm spacing for samples S1, S3, and S4 are presented in Table 2. Analogous to the porosity volume fraction and grain size, the secondary dendrite arm spacing also increases from S1 to S3 to S4, although essentially equivalent for the latter two. Previous work has examined the microstructure of cast Mg–Al alloys subjected to various solidification conditions [7]. Die cast Mg–Al alloys containing about 6% Al (AM60) were found to have a secondary dendrite arm spacing between 10 and 25 μm consistent with the present results (Table 2).

3.3. Fatigue crack formation

The overall fracture surfaces of samples S1–S4 are presented in Fig. 4. In Fig. 4, the number of cycles to failure is indicated beneath the corresponding sample number. An arrow indicates the location of the fatigue crack nucleation sites on individual samples. Sample S4 has multiple arrows highlighting a large region on the fracture surface covered by subsurface trapped oxides. The extremely low number of cycles to failure of sample S4 is undoubtedly linked to these trapped oxides, which are found over nearly a third of the fracture surface. The sites where fatigue cracks formed in samples S1, S2, and S3 are much more isolated by comparison, as shown by higher magnification images in Fig. 5. In samples S1 and S2, nucleation of the dominant fatigue crack formed at near-surface trapped oxides (Fig. 5(a) and (b)). The sizes of the trapped oxides were approximately 400 and 800 μm for the S1 and S2 samples, respectively. In sample S3, near surface fatigue cracks formed within a region of dispersed porosity that spanned a range of approximately 700 μm (Fig. 5(c)).

3.4. Fatigue crack growth and fracture

Although the fatigue crack formation sites were noticeably different for samples S1–S4, the mechanisms of fatigue crack growth and final fracture were indistinguishable between specimens as characterized with the SEM. Consequently, only representative SEM images of the fatigue and fracture mechanisms from sample S1 are presented. The mechanisms presented in this section apply to the other samples as verified by auxiliary SEM work. Fig. 6 is an image of the overall fracture surface of sample S1 with indicators of three regions to be examined in detail with the SEM. The schematic above the SEM image in Fig. 6 indicates the maximum stress intensity factor, K_{max} , for a through-edge crack subjected to a uniform tensile stress amplitude, $\Delta\sigma/2$, of 34 MPa

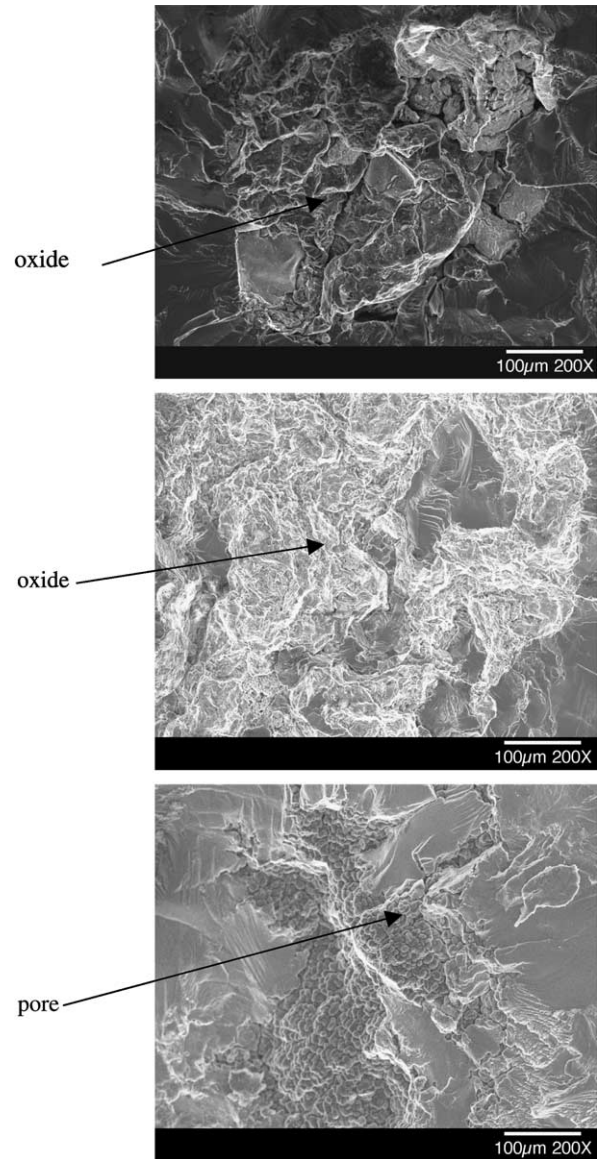


Fig. 5. High magnification images of fatigue crack formation sites for samples (a) S1, (b) S2, and (c) S3.

($E = 45 \text{ GPa}$, $\Delta\sigma/2 = 0.075\%$) [19]. The K -solution is only valid up to a crack length to specimen width ratio of 0.6. Figs. 7–10 present high magnification SEM images of Regions 1–3 indicated in Fig. 6.

Close to the crack formation site, the fracture surface in Region 1 is characterized by an extremely flat region (Fig. 7(a)) covered in fine fatigue striations (Fig. 7(b) and (c)). Due to the granular and dendritic structure in the cast Mg, local disruptions in the crack path are observed at different locations in Region 1. However, the cracks tend to preferentially grow in a microscale Mode I fashion cutting straight across the soft dendrite cells and grains. If the fatigue cracks followed the grain boundaries, interdendritic arms, or second phases, a roughness on the order of the average grain size

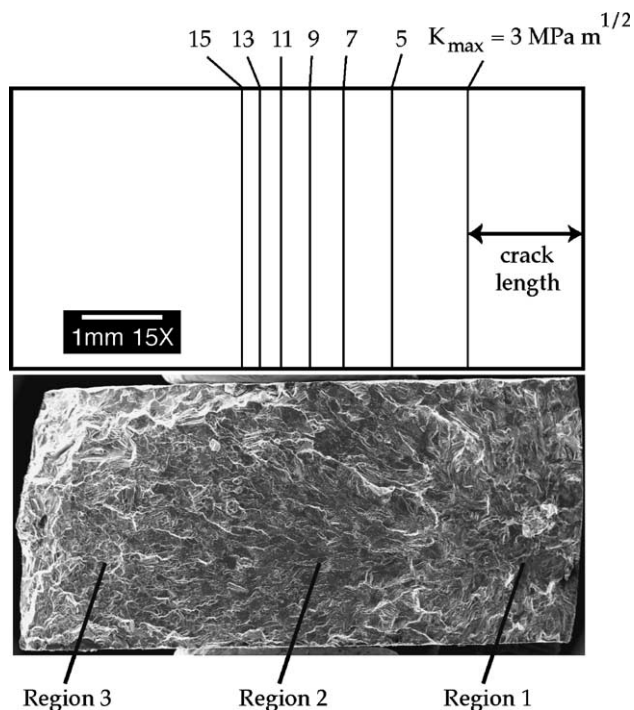


Fig. 6. Overall fracture surface of sample S1 indicating the different regions inspected with SEM. The schematic above indicates the maximum stress intensity factor for a through-thickness edge crack subjected to a uniform tensile stress amplitude, $\Delta\sigma/2$, of 34 MPa ($E = 45$ GPa, $\Delta\varepsilon/2 = 0.075\%$).

(100 μm) or dendrite cell size (15 μm) would be apparent in Fig. 7(a). On the contrary, the striated flat regions cover flat areas extending several hundreds of μm 's with small perturbations in growth at the boundaries.

In Region 2, the fatigue crack path changes to reveal a more faceted and serrated fracture surface (Fig. 8). The large facets are on the order of the grain size in this cast Mg (Fig. 8(a)), while smaller features reveal a serrated fracture mechanism in contrast to continuous fatigue striations through a homogeneous material (Fig. 8(b)). Although the advancing fatigue crack still follows a Mode I path on the macroscale, the microscale path has a preferential path through the microstructure different than the flat path through the homogeneous dendrite cells as observed in Region 1. A similar observation has been made on the fracture surface of cast AM60 Mg in the fatigued regions farther from the crack nucleation site [20]. Even farther from the fatigue crack nucleation site, in Region 3, the fracture surface has an extremely rough appearance (Fig. 9(a)) with clear evidence of overload failure mechanisms on the microscale (Fig. 9(b)). Backscatter SEM images show a notably higher fraction of second phase particles in Region 3 (Fig. 10(b)) compared to Region 1 (Fig. 10(a)), consistent with the propensity of second phase particles to facilitate the nucleation, growth, and coalescence of voids during monotonic overload failure.

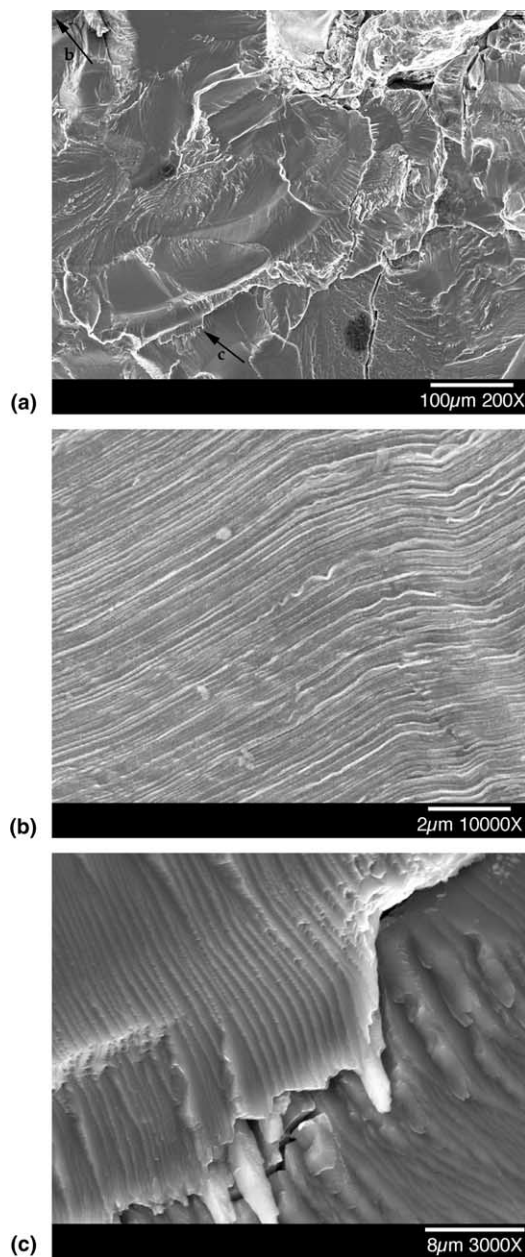


Fig. 7. Secondary SEM images from Region 1 in Fig. 6. Region 1 is characterized by a very flat surface covered by fine fatigue striations. The arrowheads in (a) indicate the locations of images (b) and (c).

4. Discussion

Based on the present experimental observations, the fatigue life in cast Mg may be influenced by the following microstructural features:

1. Largest inclusion/pore size
2. Porosity volume fraction
3. Secondary dendrite arm spacing
4. Grain size

The cast Mg material in this study exhibited poor HCF resistance because of the relatively high values (compared to cast aluminum for example) for all of the

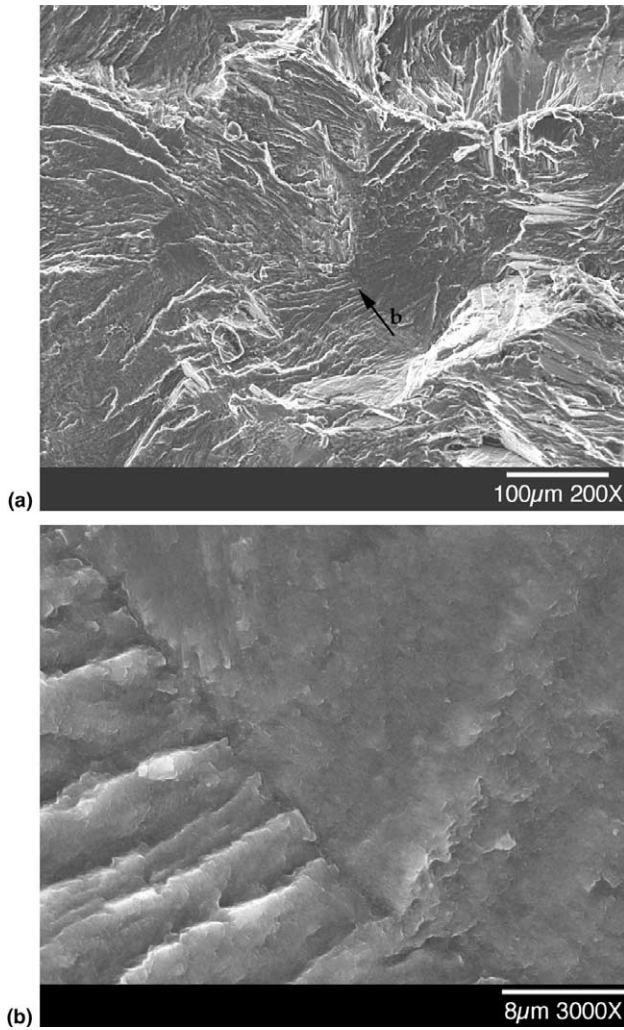


Fig. 8. Secondary SEM Images from Region 2 in Fig. 6. Region 2 is characterized by faceted surfaces and serrated growth patterns. The arrowhead in (a) indicates the location of image (b).

parameters listed above. However, this observation does not necessarily imply that the resistance to fatigue scales inversely with each parameter, or that the parameters have equivalent importance on the resistance to fatigue. In fact, some of the above microstructural features scale together due to solidification mechanisms and a particular parameter may possibly have a negligible influence on the fatigue performance. Separating the influence of the above parameters in a quantitative fashion requires elimination of specific variables via systematic experimentation [21] or micro-mechanical finite element modeling [22,23] as has been undertaken for cast Al–Si materials. In the discussion that follows a rationale is presented for including or excluding these microstructural features in predicting fatigue life of cast Mg alloys.

Significant experimental evidence shows that fatigue life correlates inversely with the size of the fatigue crack nucleation inclusion/pore in both as-cast [24,25] and wrought materials [26]. Micro-mechanical finite element

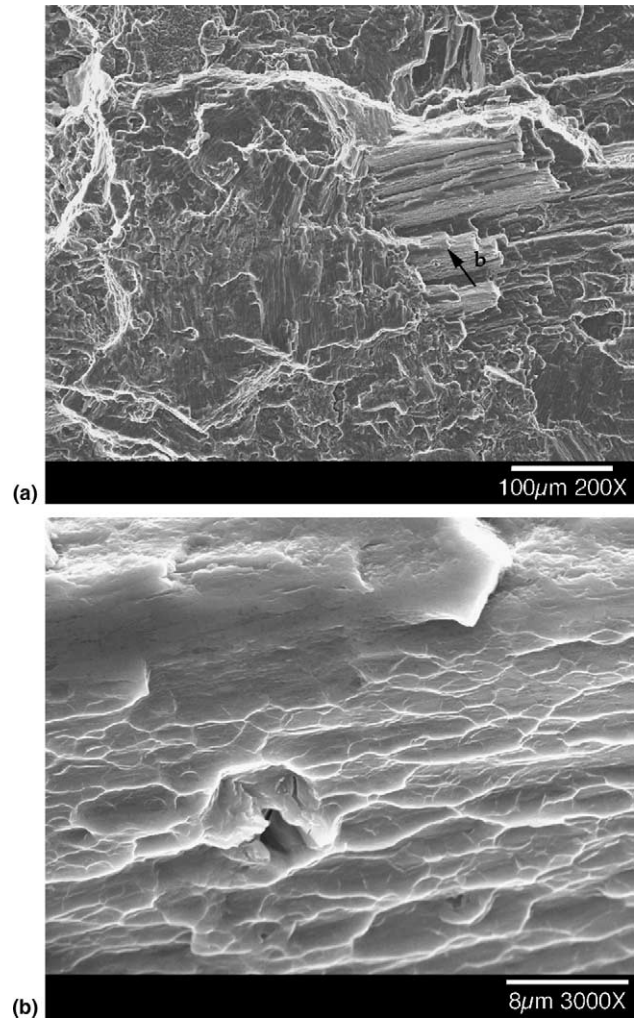


Fig. 9. Secondary SEM Images from Region 3 in Fig. 7. Region 3 is characterized by an extremely rough surface with clear indications of ductile tearing. The arrowhead in (a) indicates the location of image (b).

simulations exist to confirm that the driving force for fatigue crack nucleation from voids and inclusions increases with inclusion size [23]. The size of the fatigue crack nucleation sites in the cast Mg samples varied from several hundred microns to several millimeters as the fatigue life spanned three orders of magnitude (Fig. 4). In the worst case, distributed fatigue crack formation sites in the form of oxides spanned nearly a third of the specimen cross sectional area, resulting in a representative HCF life of just over 6000 cycles. Further evidence of the effect of nucleation site size on fatigue life can be ascertained by comparing samples S1 and S2. The samples have significantly different lives (Fig. 1) but also oxide crack nucleation sites that differ in size by a factor of two, 400 versus 800 μm (Fig. 5). The size of the porosity crack nucleation site in samples S3 is about 700 μm , nearly the size of the site in samples S2.

Based on our observations and those in the literature [13], the inclusion size appears that the fatigue crack

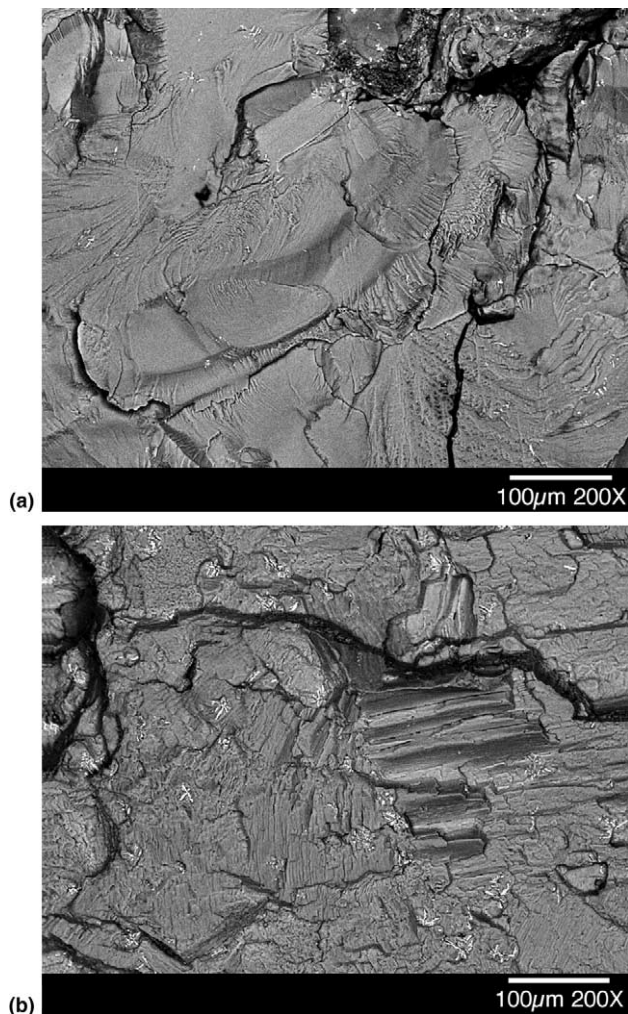


Fig. 10. Backscatter SEM Images from (a) Region 1 and (b) Region 3 in Fig. 7. The image from Region 3 shows a notably higher fraction of MnAlSi particles.

formation has a first-order influence on the HCF performance of cast Mg. Larger inclusions have a tendency to form cracks earlier due to more widespread plasticity [23] and also facilitate a larger initial crack size at the onset of propagation. Porosity and oxides both serve as preferential sites for fatigue crack formation; thus, both should be avoided in high stress regions of the casting. When porosity and/or oxide formation are unavoidable, macroscale modeling must be used to quantify fatigue crack nucleation life from such inhomogeneities, if they are detectable or predictable using solidification modeling. Commensurate with the present results, the macroscale modeling must account for the size of the inclusions. Micro-mechanical finite element modeling can be used to shed light on fatigue crack formation at inhomogeneities in cast Mg as a function of R -ratio and strain amplitude [23].

The volume fraction of pores (porosity) has long been considered an important factor in determining the strength and ductility of as-cast materials under mono-

tonic loading. Strong correlation is often reported between porosity and tensile ductility for Al–Mg–Si alloys [27]. But under HCF loading conditions, the volume fraction of porosity does not always correlate strongly with fatigue performance for Al–Si [28]. Rather, the fatigue life correlates better with the maximum pore/inclusion size [21,25] if large pores exist. If the pore size distribution remains the same and pores are spatially well distributed, HCF crack initiation and growth mechanisms might then be affected significantly by the volume fraction of porosity. In the cast Mg samples, the average porosity was observed to increase (Fig. 2) as the sample lives decreased. However, the maximum pore sizes and distributions in specimens S1, S3 and S4 were quite different.

Secondary dendrite arm spacing and grain size are microstructural features that have been shown to influence the overall fatigue life of cast materials. However, one difficulty is that both the volume fraction of pores [29] and maximum pore size [21] scale inversely with the cooling rate, as does the secondary dendrite arm spacing and grain size. Consequently, the HCF performance of a material with a relatively large secondary dendrite arm spacing and grain size will invariably be poor due to the presence of large pores which facilitate rapid fatigue crack formation and large initial crack sizes for propagation. However, unlike well-spaced large pores, the more periodic dendrite and grain boundaries can have an impact on fatigue performance via crack growth acceleration and retardation, particularly when the cracks are microstructurally small. For example, previous studies of fatigue crack growth in cast Al–Si alloys have clearly shown that the particle laden interdendritic regions act as barriers to small fatigue crack propagation [31] and hence decelerate small fatigue cracks [32]. Since a significant portion of the fatigue life can be spent during small fatigue crack propagation, the dependence of fatigue crack growth rate on the strength and period of such barriers is important.

The present experimental results show that fatigue cracks generally propagate in cast Mg via two different mechanisms, as shown in Figs. 7 and 8. Close to the nucleation site the cracks cut straight across the dendrites and grains leaving a very flat fracture surface on the microstructural scale (Fig. 7). As the crack length increases, the maximum crack tip driving force also increases as shown in Fig. 6. At a higher crack tip driving force, the fatigue cracks follow a more faceted and serrated fatigue crack path on the microstructural scale (Fig. 8). On the macroscale, the transition between the two growth patterns occurs around a maximum crack tip stress intensity factor of about $3.5 \text{ MPa} \sqrt{\text{m}}$ at the center of the specimen, which exists under a plane strain state (Fig. 7). Our elastic analysis for the stress intensity is valid, since the applied stress is 35 MPa and the yield stress is approximately 142 MPa [18]. A transition value

near $3.5 \text{ MPa} \sqrt{\text{m}}$ was also discovered during the fatigue crack growth of circular flaws in cylindrical samples of cast AM60 Mg [20]. Fatigue crack growth rate curves for cast AZ91 Mg plotted against the stress-intensity factor range [18] indicate that $3.5 \text{ MPa} \sqrt{\text{m}}$ is at the transition between near threshold and Paris law fatigue crack growth regimes. Goodenberger and Stephens [18] performed those tests under $R = 0, -1, \text{ and } -2$. A similar transition of fatigue crack growth mechanism has been observed in numerous wrought alloys [33]. The transition behavior in wrought materials is attributed to the point when the crack tip damage zone reaches the size scale of pertinent microstructural inhomogeneities such as the grain size or second phase particles [33].

Cast Mg alloys contain a significant amount of heterogeneities such as pores, grain boundaries, dendrite arms and cells, and second phases. Results in this study have shown that the transition in growth modes corresponds to a change in fatigue crack growth mechanism from striated growth through the cells to serrated growth across interdendritic regions or grain boundaries. Consequently, the growth transition in cast Mg depends on the ability of the crack tip process zone to sample a statistically significant fraction of heterogeneous features that comprise the interdendritic regions or grain boundaries. For a cast Mg material with a yield strength, σ_y , of 142 MPa [18] and a transition stress intensity factor of $3.5 \text{ MPa} \sqrt{\text{m}}$, the maximum process zone size can be approximated in plane strain as [19]:

$$r_y = \frac{1}{6\pi} \left(\frac{K_{\max}}{\sigma_y} \right)^2 \approx 32 \text{ } \mu\text{m}. \quad (1)$$

A maximum process zone of $32 \text{ } \mu\text{m}$ is approximately twice the average secondary dendrite arm spacing and a third of the average grain size in the sample S1 of cast Mg (Table 2). Consequently, the transition in growth mechanisms corresponds to a switch in growth mechanisms from across the dendrite cells to growth through interdendritic regions, as also observed in cast Al–Si alloys [30,31]. The interdendritic regions are decorated with second phases such as $\beta\text{-Al}_{12}\text{Mg}_{17}$ particles, which can fracture and debond ahead of the crack tip at higher crack tip driving forces, creating preferential path for fatigue crack advance under overload conditions.

The fatigue crack growth mechanisms identified here have ramifications for the development of microstructure-based life prediction models for cast Mg. To develop such models, future work is necessary to quantify trends in fatigue crack growth with the microstructure. Aside from the fatigue crack formation/initiation sites, pores and oxides were not discovered in the fatigued region of the fracture surface. Although it is certainly possible for a fatigue crack to cross a pore or an oxide, the present findings indicate that they may not be critical in fatigue crack growth, although they can assist fatigue crack formation. On the contrary, the dendrite constit-

uents (aluminum, intermetallics, etc.) shelve a large influence on the path of fatigue cracks and consequently the fatigue crack growth rates during cycling. Future micro-mechanical modeling efforts must focus on understanding the explicit role that the dendrite boundaries play on crack growth retardation at small crack sizes. Specific work should focus on quantifying the effect of secondary dendrite arm spacing on crack propagation rates.

5. Conclusions

Samples of cast Mg machined from a commercial high-pressure automotive die-casting were tested until failure under completely reversed cycling in laboratory air at room temperature at strain amplitudes ranging from 0.02% to 0.5%. Initial microstructures and fracture surfaces of the failed samples were examined with SEM, and the following observations support these primary conclusions:

- (I) The variability in the fatigue life data in the HCF regime spans over two orders of magnitude. The difference in lives for the specimens machined from the casting is primarily attributed to a difference in the inclusion size that start fatigue cracks, which range from several mm to several hundred μm . Secondary effects may include the influence of average secondary dendrite arm spacing and average grain size, which were found to vary from 15–22 and 105–140 μm , respectively. The average secondary dendrite arm spacing and grain size can influence fatigue crack propagation rates, particularly in the microstructurally small fatigue crack regime (cf. [34]).
- (II) At low crack tip driving forces for completely reversed straining ($K_{\max} < 3.5 \text{ MPa} \sqrt{\text{m}}$), intact particles and boundaries can act as barriers to fatigue crack propagation, and consequently the cracks will tend to avoid the interdendritic regions and progress through the relatively homogeneous dendrite cell interiors, leaving a fine striated pattern in this single-phase region. At high driving forces that correspond to overload conditions ($K_{\max} > 3.5 \text{ MPa} \sqrt{\text{m}}$), fractured particles and inclusion debonding can create weak paths for fatigue crack propagation, and consequently the cracks will follow the interdendritic regions and leave serrated markings.

Acknowledgements

This work has been sponsored by the US Department of Energy, Sandia National Laboratories under contract DE-AC04-94A185000. This work was performed under

the auspices the USCAR Lightweight Metals Group (Dick Osborne and Don Penrod, project technical monitors). We would like to thank Westmoreland Mechanical Testing and Research for conducting the fatigue tests and N. Li and G. Cole at Ford Motor Company for the cast Mg automotive component. J. Chames and A. Gardea from Sandia are gratefully thanked for microscopy assistance. The work of M.F. Horstemeyer is also funded by the Mississippi State University Center for Advanced Vehicular Systems.

References

- [1] Jambor A, Beyer M. New cars – new materials. *Mat Des* 1997;18:203–9.
- [2] Decker RF. The renaissance in magnesium. *Adv Mater Proc* 1998;154:31–3.
- [3] Froes FH, Eliezar D, Aghion E. The science, technology, and applications of magnesium. *JOM* 1998;September:30–4.
- [4] Lunder O, Aune TK, Nisancioglu K. Effect of Mn additions on the corrosion behavior of mould-cast magnesium ASTM AZ91. *Nat Ass Corr Eng* 1987;43:291–5.
- [5] Song G, Atrens A, Dargusch M. Influence of microstructure on the corrosion of diecast AZ91D. *Corros Sci* 1999;41:249–73.
- [6] Ambat R, Aung NN, Zhou W. Evaluation of microstructural effects on corrosion behavior of AZ91D magnesium alloy. *Corros Sci* 2000;42:1433–55.
- [7] Carlson BE. Influence of processing variables and aluminum content on the microstructure and mechanical properties of cast Mg–Al Alloys. Ph.D. Dissertation, University of Michigan, Ann Arbor, MI, 1997.
- [8] El-Mahallawy NA, Taha MA, Pokora E, Klein F. On the influence of process variables on the thermal conditions and properties of high pressure die-cast magnesium alloys. *J Mater Process Technol* 1998;73:125–38.
- [9] Miller WK. Creep of die cast AZ91 magnesium at room temperature and low stress. *Met Trans A* 1991;22:873–7.
- [10] Gutman EM, Unigovski Ya, Levkovich M, Koren Z, Aghion E, Dangur M. Influence of technological parameters of permanent mold casting and die casting on creep and strength of Mg alloy AZ91D. *Mater Sci Eng A* 1997;234:880–3.
- [11] Yue TM, Ha HU, Musson NJ. Grain size effects on the mechanical properties of some squeeze cast light alloys. *J Mater Sci* 1995;30:2277–83.
- [12] Mabuchi M, Kubota K, Higashi K. Tensile strength, ductility, and fracture of magnesium-silicon alloys. *J Mater Sci* 1996;31:1529–35.
- [13] Lee S, Lee SH, Kim DH. Effect of Y, Sr, and Nd additions on the microstructure and microfracture mechanism of squeeze-cast AZ91-X magnesium alloys. *Met Trans A* 1998;29:1221–35.
- [14] Han BQ, Dunand DC. Microstructure and mechanical properties of magnesium containing high volume fraction of dispersoids. *Mater Sci Eng A* 2000;277:297–304.
- [15] Strizhalo VA, Khilchevskii VV, Chernyi AA, Fedorin AM, Baumshtein MV. Fracture anomaly of cast magnesium alloys under low-cycle fatigue. *Str Mater* 1983;15:898–901.
- [16] Llorca N, Bloyce A, Yue TM. Fatigue behavior of short alumina fibre reinforced AZ91 magnesium alloy metal matrix composite. *Mater Sci Eng A* 1991;135:247–52.
- [17] Perov SN, Ogarevic VV, Stephens RI. Application and verification of fatigue life calculation methods for AZ91E-T6 cast magnesium alloy under variable amplitude loading. *ASME J Eng Mater Technol* 1993;115:385–90.
- [18] Goodenberger DL, Stephens RI. Fatigue of a AZ91E-T6 cast magnesium alloy. *ASME J Eng Mater Technol* 1993;115:391–7.
- [19] Ewalds HL, Wanhill RJH. *Fracture mechanics*. London: Edward Arnold; 1984.
- [20] Horstemeyer MF, Yang N, Gall KA, McDowell DL, Fan J, Gullett P. High cycle fatigue mechanisms in a cast AM60B magnesium alloy. *Fat Fract Eng Mater Struct* 2002;25:1–12.
- [21] Major JF. Porosity control and fatigue behavior in A356-T61 aluminum alloy. *AFS Trans* 1994;102:901–6.
- [22] Gall K, Horstemeyer MF, McDowell DL, Fan J. Finite element analysis of the stress distributions near damaged Si particle clusters in cast Al–Si alloys. *Mech Mater* 2000;32:277–301.
- [23] Gall K, Horstemeyer MF, Degner BW, McDowell DL, Fan J. On the driving force for fatigue crack formation from inclusions and voids. *Int J Fract* 2001;108:207–33.
- [24] Ting JC, Lawrence FV. Modeling the long-life fatigue behavior of a cast aluminum alloy. *Fat Fract Eng Mater Struct* 1993;16:631–47.
- [25] Zhang B, Poirier DR, Chen W. Microstructural effects on high-cycle fatigue-crack initiation in A356.2 casting alloy. *Metall Trans* 1999;30A:2659–65.
- [26] Murakami Y, Endo M. Effects of defects, inclusions, and inhomogeneities on fatigue strength. *Int J Fatigue* 1994;16:163–82.
- [27] Caceres CH, Selling BI. Casting defects and the tensile ductility of an Al–Mg–Si alloy. *Mater Sci Eng* 1996;A220:109–16.
- [28] Sonsino CM, Ziese J. Fatigue Strength and applications of cast aluminum alloys with different degrees of porosity. *Int J Fatigue* 1993;15:75–84.
- [29] Wickberg A, Gustafsson G, Larsson L-E. Microstructural effects on the fatigue properties of a cast Al7SiMg alloy. *SAE Trans* 1984;840121:1.728–35.
- [30] Gall K, Yang N, Horstemeyer MF, McDowell DL, Fan J. The debonding and fracture of Si particles during the fatigue of a cast Al–Si alloy. *Met Trans A* 1999;30:3079–88.
- [31] Gall K, Yang N, Horstemeyer MF, McDowell DL, Fan J. The influence of modified intermetallics and Si particles on fatigue crack paths in a cast A356 al alloy. *Fract Eng Mater Struct* 2000;23:159–72.
- [32] Shiozawa K, Tohda Y, Sun S-M. Crack initiation and small fatigue crack growth behavior of squeeze-cast Al–Si aluminum alloys. *Fat Fract Eng Mater Struct* 1997;20:237–47.
- [33] Suresh S. *Fatigue of materials*. Cambridge, UK: Cambridge University Press; 1991.
- [34] McDowell DL, Gall K, Horstemeyer MF, Fan J. Microstructure-based fatigue modeling of cast A356-T6 alloy. *Eng Fract Mech* 2003;70:49–80.